Multi Time-Scale Modeling of a STATCOM and Power Grid for Stability Studies using Modelica

Marcelo de Castro
Rensselaer Polytechnic Institute
Troy, NY, USA
Email: decasm3@rpi.edu

Luigi Vanfretti
Rensselaer Polytechnic Institute
Troy, NY, USA
Email: vanfrl@rpi.edu

***Abstract*—Currently many power-electronic-based devices are being connected to the electric power grid. An efficient way to study the interaction between these devices' controllers, and the resulting electromagnetic and electromechanical responses is to use hybrid wave-phasor simulations. Many solutions involving the co-simulation of electromagnetic (EMT) and transient stability (TS) models have been proposed in literature, with different techniques being employed for the calculation of a phasor from the wave quantities. This paper presents a Modelica implementation of a hybrid interface that enables the coupling of two portions of a power grid, with each portion defined in models in two different time-scales. The interface is used in Modelica-compliant environment to interface a STATCOM, as an EMT model, with a single machine infinite bus system, as the phasor model. Results to assess the interface performance and the STATCOM implementation are presented.**

I. Introduction

In the last few decades the electric power system has grown in size and complexity. Many different devices based on power-electronics technologies have been connected to the grid since the second half of the 20th century. High Voltage Direct Current (HVDC) transmission lines and Flexible AC Transmission Systems (FACTS) devices [1] have been operating for decades now and recent improvements in switching devices has bolstered the connection of new power electronics devices to the bulk power system. Furthermore, owing to the global growth of environmental concerns, alternative energy sources such as wind and solar are now abundant in the grid. These renewable sources are, very frequently, interfaced through a power electronic converter, making these ubiquitous devices to be incredibly important for the study of power systems.

Indeed, stability studies involving electromechanical, electromagnetic and control dynamics are an essential assessment for the safe operation of power systems [2]. Transient Stability (TS) programs focus on electromechanical behavior considering only the positive sequence phasor equivalent components at the fundamental frequency for the entire system. Low-order numerical integrators (i.e. Euler and Trapezoidal methods) are employed to perform the simulations that are needed for the study of TS problems allowing a large number of equations to be solved with relatively high speed [2], [3]. On the other hand, ElectroMagnetic Transient (EMT) programs use models that are usually discretized using Dommel's method [4]. In these simulations, equations are solved over a large frequency bandwidth and, therefore, the solvers need to take into account ultra-fast frequencies using very small time-steps. Solving these equations demands a considerable amount of time, limiting its application for large-scale power systems.

Since the 80s, the need for hybrid EMT-TS simulation was evident due to studies to understand the interactions of HVDC converters and the power grid [8], [9]. There, the HVDC link and its converters are modeled and simulated in an EMT approach, while the rest of the system is represented with its TS equivalent. The interface between systems is performed using the Fast Fourier Transform (FFT) or Curve Fitting (CF) algorithms [6]. Recently, co-simulation strategies have been proposed in which Phase-Locked Loop (PLL) and Double Second Order Generalized Integrator (DSOGI) band-pass filters for the extraction of positive-sequence fundamental component phasors [10]–[12]. These strategies have shown great potential, especially in terms of computational efficiency during simulation and interested readers are referred to [11] for a detailed comparison between full-EMT and hybrid simulations.

However, models created for the simulation of such systems are usually linked to the numerical solver used for the solution, i.e. they are discretized and described using a specific numerical scheme. In contrast, models developed in this paper are separated from the numerical solvers by using the Modelica language [13], allowing the use of both fixed-step and/or advanced variable-step DAE solvers [15]. By unifying the models under an equation-based approach as a modeling paradigm, makes it unnecessary the usage of two separate modeling environments, numerical algorithms or specific discretization of the model's equations. It also allows symbolic-based linearization of the combined EMT-TS system, and to apply control design tools directly in the same environment where the hybrid simulation is carried out, which is unique and goes beyond the state-of-the art of modeling and simulation tools for power systems.

In this context, this work presents preliminary work on modeling and implementation of the hybrid interface proposed in [11] using Modelica as an equation-based modeling language.

This work was funded in part by the CURENT ERC, in part by the New York State Energy Research and Development Authority (NYSERDA) under grant agreement numbers 37951, in part by Dominion Energy, and in part by the Center of Excellence for NEOM Research at King Abdullah University of Science and Technology.

The hybrid interface is used to perform a simulation study of a interconnection of a detailed, switched model of a STATCOM into a phasor-based network model. Both power system models are also implemented in Modelica. The STATCOM and its controllers are assembled using dedicated component models and the Modelica Standard Library, while the power system phasor-based model is built using the OpenIPSL [17].

The remainder of this paper is structured as follows: Section II brings the description and the fundamentals about the hybrid interface. Section III describes the STATCOM model. Section IV briefly presents the development needed for designing the STATCOM controllers. Section V brings the studied test system. Section VI presents the results and conclusions are presented in Section VII.

II. Hybrid Wave-to-Phasor Interface Description

The integration between models created under different paradigms, i.e. EMT-and-TS-like models, requires a component able to adequately interface both systems. Usually, the two systems exchange information using a co-simulation approach, which is different from what is presented herein. In this paper, the interface component is implemented following the DSOGI filter first used for co-simulation in [10]–[12]. In simple words, the TS-like system with phasor-based models acts similar to a variable voltage source at the interface bus. The transformation of the voltage phasor to a wave-like voltage source requires a phasor-to-wave transformation. On the other hand, the EMT models acts as a variable current injection on the interface bus. This phasor-type current injection must be calculated from the wave-equations obtained from the detailed EMT-like system and, thus, a wave-to-phasor transformation is needed. Figure 1 depicts the scheme of transformations necessary for the interface.

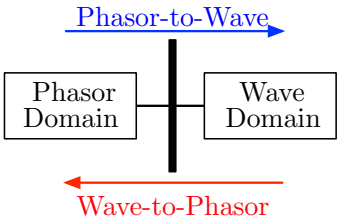

Fig. 1: Simplified diagram for the wave-phasor interface.

A. Voltage phasor-to-wave

This interface takes information from the phasor such as phase, amplitude and frequency and translates it to waveform equations. The phasor can be interpreted as the representation of a sinusoidal signal $y(t)$ as a complex number $\tilde{Y}$ from Euler's relation. Hence, consider the signal given by

$$y(t) = A\sqrt{2}\cos\left(\omega t + \phi\right). \tag{1}$$

The phasor representation of signal $y(t)$ is shown in Eq. (2) below. The magnitude A of phasor $\tilde{Y}$ is, actually, the Root Mean Squared (RMS) value of the signal $y(t)$. In addition, it is important to observe that information about the frequency ω is implicit in the phasor representation.

$$\tilde{Y} = A\angle\phi = A\left(\cos\phi + j\sin\phi\right) \tag{2}$$

Figures 2a and 2b depict the graphical representation of the signal $y(t)$ in its time representation and in its phasor representation, respectively.

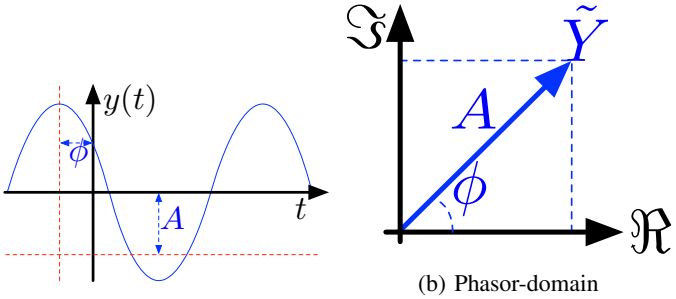

(a) Time-domain representation.

(b) Phasor-domain representation.

Fig. 2: Different representations of sinusoidal signal $y(t)$.

The interface is implemented in Modelica, using OpenIPSL [17] and, therefore, it is necessary to understand how the phasor information is carried through the `connector` Modelica concept [14]. The connector in OpenIPSL is called `PwPin` and has two variables describing the voltage phasor and two others for the current phasor, declared as `flow` variable. However, only the voltage will use the phasor-to-wave interface. Phasor quantities, in OpenIPSL are presented in Cartesian coordinates and, thus, written as:

$$\tilde{V} = v_{re} + jv_{im}. \tag{3}$$

Hence, it is possible to calculate the wave from the phasor interface using Equation (3).

$$\begin{cases} A = \sqrt{v_{re}^2 + v_{im}^2}, \\ \phi_v = tg^{-1}\left(\dfrac{v_{im}}{v_{re}}\right), \\ \omega_s = \omega_0 + \dfrac{d\phi_v}{dt}. \end{cases} \tag{4}$$

where ω_s is an estimate of the wave's frequency and $\omega_0 = 2\pi \times 60$. The calculated phase ϕ is assumed to be the phase ϕ_A from phase A's voltage. Since the positive sequence model assumes that there is no unbalance, the phases of voltages in B and C can be calculated by a simple displacement of $\frac{2\pi}{3}$ radians. Finally, it is possible to write that:

$$\begin{cases} v_a = A\sqrt{2}\cos\left(\omega_s t + \phi\right), \\ v_b = A\sqrt{2}\cos\left(\omega_s t + \phi - \dfrac{2\pi}{3}\right), \\ v_c = A\sqrt{2}\cos\left(\omega_s t + \phi + \dfrac{2\pi}{3}\right). \end{cases} \tag{5}$$

B. Current wave-to-phasor

This interface requires additional computations compared to the previous one because a filtering process is needed. In this work, a DSOGI [18] is used in order to extract the positive sequence component out of the fundamental frequency signal. It is important to understand how to use the filtering process to extract the positive sequence. First, consider the vector of three-phase instantaneous quantities $\mathbf{i_{abc}}$ and the vector of three-phase positive-sequence instantaneous components $\mathbf{i^+_{abc}}$. The relationship between them can be written as [11]:

$$\mathbf{i^+_{abc}} = \begin{bmatrix} i_a^+ \\ i_b^+ \\ i_c^+ \end{bmatrix} = \left[\mathbf{T}^+\right] \mathbf{i_{abc}} = \left[\mathbf{T}^+\right] \begin{bmatrix} i_a \\ i_b \\ i_c \end{bmatrix}. \tag{6}$$

where

$$\left[\mathbf{T}^+\right] = \frac{1}{3} \begin{bmatrix} 1 & a & a^2 \\ a^2 & 1 & a \\ a & a^2 & 1 \end{bmatrix}, \tag{7}$$

and $a = e^{j\frac{2\pi}{3}}$ is a phase displacement operator. Then, it is possible to write the vector $\mathbf{i_{abc}}$ in terms of the Clarke reference frame, i.e., $\mathbf{i}_{\alpha\beta}$. Hence:

$$\begin{aligned} \left[\mathbf{T}_{\alpha\beta}\right] \mathbf{i^+_{abc}} &= \left[\mathbf{T}_{\alpha\beta}\right] \left[\mathbf{T}^+\right] \mathbf{i_{abc}}, \\ \mathbf{i}^+_{\alpha\beta} &= \left[\mathbf{T}_{\alpha\beta}\right] \left[\mathbf{T}^+\right] \left[\mathbf{T}_{\alpha\beta}\right]^{-1} \mathbf{i}_{\alpha\beta}, \\ \mathbf{i}^+_{\alpha\beta} &= \frac{1}{2} \begin{bmatrix} 1 & -q \\ q & 1 \end{bmatrix} \mathbf{i}_{\alpha\beta} \end{aligned} \tag{8}$$

where $q = e^{j\frac{\pi}{2}}$ is an orthogonal phase displacement operator and

$$\left[\mathbf{T}_{\alpha\beta}\right] = \frac{2}{3} \begin{bmatrix} 1 & -\frac{1}{2} & -\frac{1}{2} \\ 0 & \frac{\sqrt{3}}{2} & -\frac{\sqrt{3}}{2} \end{bmatrix}. \tag{9}$$

To obtain the quadrature signals in the $\alpha\beta$ reference frame, it is possible to use one SOGI filter in each axis (α and β) right after a block that calculates the Clarke transformation. The structure of a SOGI filter is presented in Figure 3.

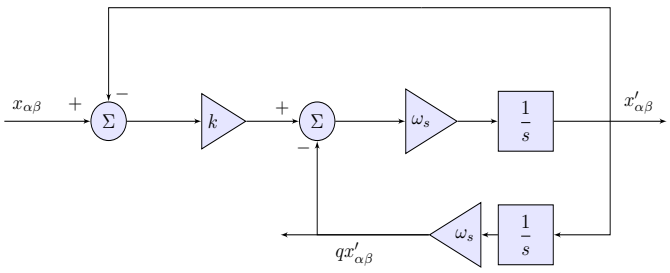

Fig. 3: Diagram representing a Second Order Generalized Integrator (SOGI).

Applying this filter, the signal $x_{\alpha\beta}$ becomes $x'_{\alpha\beta}$, in phase with the original, and $qx'_{\alpha\beta}$, a signal in quadrature with the original. The transfer functions can be described as

$$D(s) = \frac{x'_{\alpha\beta}}{x_{\alpha\beta}} = \frac{k\omega_s s}{s^2 + k\omega_s s + \omega_s^2}, \tag{10}$$

$$Q(s) = \frac{qx'_{\alpha\beta}}{x_{\alpha\beta}} = \frac{k\omega_s^2}{s^2 + k\omega_s s + \omega_s^2}, \tag{11}$$

where the gain ω_s is the angular frequency of the wave that must be filtered and it can be used as a constant gain or an adaptive gain, e.g. determined by a PLL system. In this work, the gain $\omega_s = 2\pi 60$ is constant. Note that $D(s)$ acts as a band-pass filter while $Q(s)$ is a low-pass filter. Figure 4 shows the band-pass filter performance for different gains k. In this study, an appropriate value of the gain is chosen to be $k = 1.4142$, because it has interesting properties related to the settling time and the overshoot of the filtering process undergoing disturbances [18].

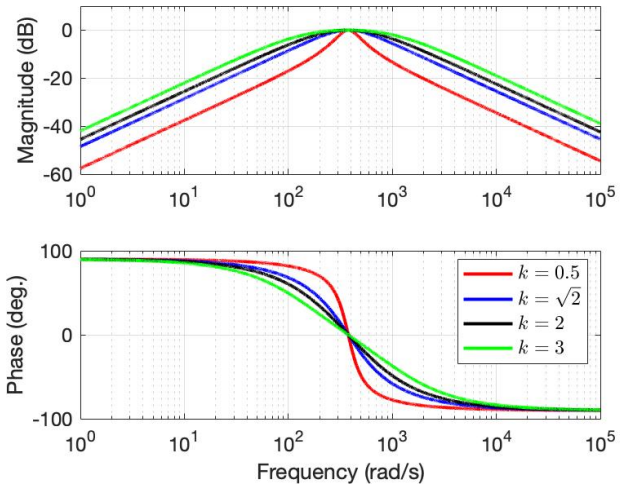

Fig. 4: Bode plot for the different gains of SOGI's band-pass filter.

Now that necessary filtering has been described, it is necessary to understand how the real and imaginary components for the current phasor are calculated. Indeed, the voltage wave, in Eq. (5) undergoes synchronization through a Synchronous Reference Frame (SRF) PLL [11]. This allows to determine the phase angle ϕ_{iv} that is needed to calculate the displacement between current and voltage phasors. The step-by-step procedure below shows how this interface extracts the current phasor from the waveforms.

1. The abc waveforms are transformed to the $\alpha\beta$ frame by applying the Clarke transformation;
2. The $\alpha\beta$ waves are filtered, individually, by a SOGI filter and the fundamental component current waveform, along with a waveform in quadrature, is obtained;
3. The positive sequence component of the $\alpha\beta$ frame is obtained;

4. The positive sequence components of $\alpha\beta$ are moved to the dq frame by applying Park's transformation, using the angle from the SRF-PLL synchronized with the voltage from Eq. (5);
5. For the current in dq frame, its angle ϕ_{iv} with relation to the reference voltage is calculated;
6. The current in dq frame is displaced by ϕ_v, scaled by current base and by its RMS value;
7. The phasor is computed as: $\tilde{I} = i_d + ji_q$.

III. STATCOM Model

The Static Compensator, or STATCOM, is a power-electronic-based device that is connected to a substation in order to compensate the reactive power or to control the substation bus terminal voltage. In this work, the model that was used was implemented in Modelica as a switching three-phase voltage-source converter (VSC). The converter's electrical diagram is shown in Figure 5. This circuit is used for modeling the controllers but it is also used as the converter model that is implemented in Modelica.

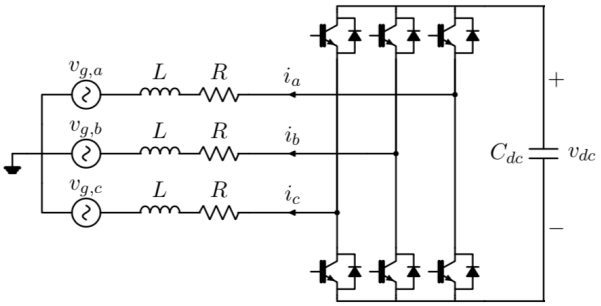

Fig. 5: STATCOM electrical circuit that is implemented in Modelica.

The dynamics of a VSC is characterized by two types of behavior. One is related to the branch that connects the STATCOM to the grid (an RL branch in this study) and the other is related to the DC voltage over the capacitor. Both are well documented in [19] and, therefore, the reader is referred to the literature for detailed information. In summary, in the dq frame it is possible to describe the dynamic behavior of the current flowing through the RL branch by:

$$\begin{cases} L\dfrac{d}{dt}i_d = -Ri_d + \omega i_q + \left(\dfrac{v_{dc}}{2}\right)m_d - v_{gd}, \\ L\dfrac{d}{dt}i_q = -\omega i_d - Ri_q + \left(\dfrac{v_{dc}}{2}\right)m_q - v_{gq}. \end{cases} \tag{12}$$

where L is the inductance, R the resistance, v_t is the converter synthesized terminal voltage and v_g is the interface bus voltage. Using the SRF-PLL, the quadrature component of the grid voltage will be equal to v_{gq} = 0. The capacitor dynamics are given by [19]:

$$\frac{C_{eq}}{2}\frac{d}{dt}(v_{dc})^2 = -\frac{3}{2}v_{gd}i_d. \tag{13}$$

IV. Control Design

The controllers are designed according to [19] and are divided into two subsections, one for the dq current controllers and one for the DC bus voltage controller.

A. Current Controller

The VSC uses a PWM strategy, hence, the relationship between the modulation indexes, m_d and m_q, and the controller outputs, u_d and u_q, are [19]:

$$\begin{cases} m_d &= \dfrac{2}{v_{dc}}\left(u_d - \omega L i_q + v_{gd}\right), \\ m_q &= \dfrac{2}{v_{dc}}\left(u_q + \omega L i_d + v_{gq}\right). \end{cases} \tag{14}$$

Therefore, the plant dynamics can be described by two decoupled responses, as the$d$ axis dynamics only depends on d variables and q axis dynamics only depends on q variables. Since dq variables have a stationary behavior, a Proportional-Integral (PI) controller is able to track the reference. The PI regulator has the following transfer function:

$$G(s) = K_p + \frac{1}{T_i s} = \frac{K_p T_i s + 1}{T_i s} \tag{15}$$

Applying this controller to act on the error between a reference (i_d^* and i_q^*) and measured signal (i_d and i_q), and by choosing $K_{p,i} \times T_i = \frac{L}{R}$, it is possible to create a zero-pole cancellation and the dynamics of the current are going to be governed by a first order transfer function.

$$C_{CL}(s) = \frac{1}{s\tau_i + 1} \tag{16}$$

where $\tau_i = \frac{L}{K_{p,i}}$. This time constant can be selected between $0.5 - 5$ ms [19]. Hence, by knowing the equivalent resistance and the inductance of the RL branch, and selecting an appropriate value of time constant τ_i, it is possible to calculate proportional gain $K_{p,i} = \frac{L}{\tau_i}$ and the integral time constant $T_i = \frac{\tau_i}{R}$.

B. DC Voltage Controller

This controller requires to perform small signal analysis as described in [19]. In addition, it is important to note that v_{dc} is controlled directly. The small signal dynamic relationship between the square of the DC bus voltage and the $d-$axis current is given by:

$$\frac{\Delta v_{dc}^2}{\Delta i_d} = -\frac{3v_{gd0}}{sC_{eq}} \tag{17}$$

where v_{gd0} is the steady state value of v_{gd} after the PLL synchronization. Using the scheme in [19], v_{gd0} has the same value as the peak magnitude of the voltage wave. It is important to recall that for this transfer function, it is assumed that the current controller placed on the $d-$axis is faster than the controller placed to generate its reference signal i_d^*. By placing a PI to generate the reference signal i^* using the error

$\left(\Delta v_{dc}^2\right)^* - \Delta v_{dc}^2$ it is possible to obtain the following closed loop dynamics:

$$\frac{\left(\Delta v_{dc}^2\right)^*}{\Delta i_d} = \frac{\frac{3K_{p,v}v_{gd0}}{C_{eq}}s + \frac{3v_{gd0}}{T_v C_{eq}}}{s^2 + \frac{3K_{p,v}v_{gd0}}{C_{eq}}s + \frac{3v_{gd0}}{T_v C_{eq}}}. \tag{18}$$

It follows that, by comparing this transfer function with a canonical second order transfer function we can determine the gains by selecting desired natural frequency ω_n and ξ for the closed loop dynamics. Hence the gains are:

$$\begin{cases} K_{p,v} = \dfrac{2\xi\omega_n C_{eq}}{3v_{gd0}}, \\ T_v = \dfrac{3v_{gd0}}{C_{eq}\omega_n^2}. \end{cases} \tag{19}$$

V. Studied System

In this paper a test system is designed to study the behavior of the interface and its applications. All models are simulated in Dymola, using variable time-step DASSL solver.

A. STATCOM

Figure 6 depicts the STATCOM implementation along with its controllers and the connection to the hybrid interface located at the left part of the image.

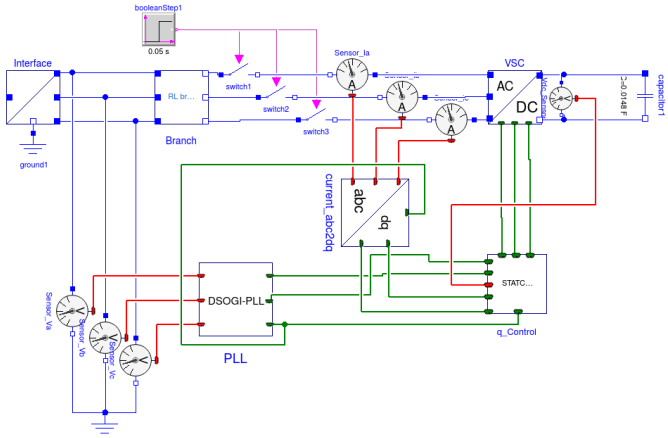

Fig. 6: Diagram for testing the STATCOM implementation and its controllers.

The parameters for the STATCOM, along with gains and time constants for its controllers and the interface filter gain are listed in the Table I. Note that the branch resistance might appear to be large, but it is chosen to be so intentionally. This makes the grid to appear weak for the STATCOM, imposing challenges to the interface in the filtering of harmonics, for example.

B. SMIB Test System

This test system was developed to study the performance of the interface and STATCOM controllers coalesced with an electromechanical power system model, i.e. a single machine infinite bus system. Figure 7 depicts the interconnection of the STATCOM to bus 2 in the SMIB system.

TABLE I: Parameters for Simulation of STATCOM.

Parameter	Description	Value	Unit
R	Branch resistance	0.1	Ω
L	Branch inductance	4.4	mH
C_{eq}	DC bus capacitor	14.8	mF
V_{dc}	DC bus voltage	60	kV
V_{line}	RMS line voltage	33	kV
k	Interface SOGI gain	1.4142	-
$K_{p,i}$	Proportional gain in i	8.8	V/A
T_i	Time constant in i	0.005	s
$K_{p,v}$	Proportional gain in v	0.07045	A/V
T_v	Time constant in v	0.60242	s

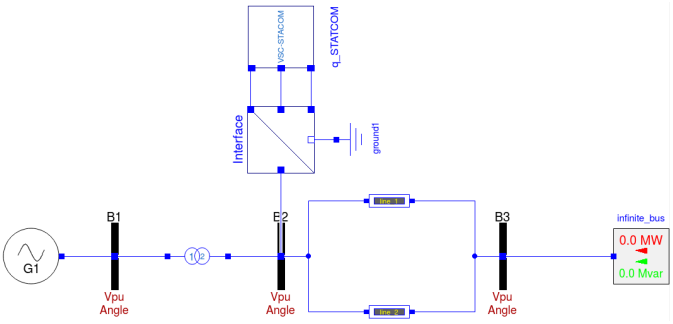

Fig. 7: Diagram for testing the STATCOM connection in SMIB system.

A value of 90 MVar is set as the reactive power reference to be injected in the grid at $t = 1$ s. The STATCOM presented in Figure 6 is encapsulated in the model named `q_STATCOM` for better visualization.

VI. Results

In this test system, two events occur. The first is the connection of the STATCOM to the grid, at $t = 0.05$ s and the second is the change of reference for reactive power to be injected into the grid. The reference changes in $t = 1$ s from 0 to 90 MVAr. The modulation indices for each phase are shown in Figure 8. Note that the modulation changes almost instantaneously at $t = 1.0$ s, showing the efficiency of the control strategy.

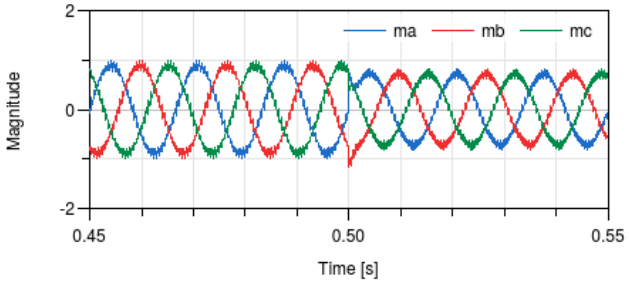

Fig. 8: Three-phase modulation signals for the VSC converter.

The behavior of the voltage over the DC capacitor can be observed in Figure 9.Once again it is possible to observe both

events in the DC voltage behavior. Also note that the maximum overshoot is less than 400 V, corresponding to less than 0.6%.

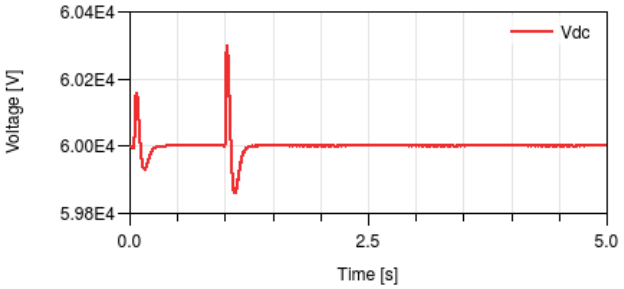

Fig. 9: STATCOM DC capacitor voltage for SMIB test.

The behavior of bus 2 voltage is presented in Figure 10. It is possible to observe that the bus voltage increases its magnitude, as it was expected due to the reactive support being offered by the STATCOM. A better result could be obtained with a terminal voltage control and this is suggested as a future work.

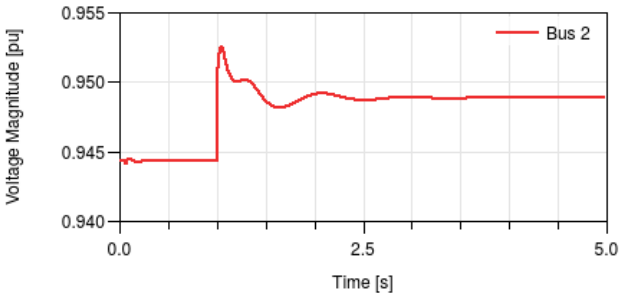

Fig. 10: Voltage magnitude behavior during simulation.

Another interesting result is the reactive power being injected into the infinite bus, which is shown in Figure 11. Note that after the STATCOM starts injecting 90 MVar, the infinite bus reduces its injection of reactive power, or it increases its reactive power consumption.

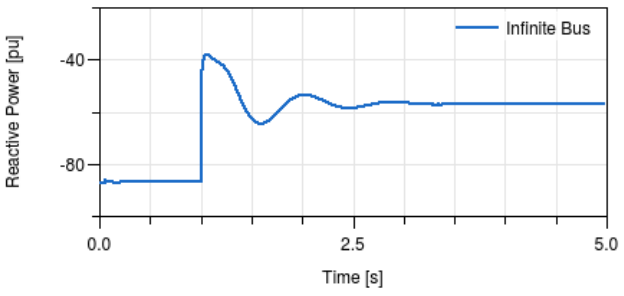

Fig. 11: Reactive power being consumed by the Infinite Bus.

VII. Conclusions

This work presented a wave-phasor interface implemented in Modelica for the coalesced simulation of hybrid EMT-TS models. The interface was built using SOGI-based filters as proposed in [11]. A full switching model of a STATCOM is implemented using Modelica and it is tested in two different simulations. The first test system example shows that the controllers are well designed and that the converter works properly. The second test system simulation shows that the hybrid wave-phasor interface can be used as a magnifying glass, allowing parts of the system to be modeled in detail (EMT) while other parts of the system are modeled with simplified models (TS).

Although the work shown in this paper brings interesting results, it is important to state that other aspects of the interface are intended to be investigated in the near future. For example, the accuracy of the frequency, and its deviation from nominal, are intended to be studied in next phases. Moreover, the "physical" connection between the two different models allow the linearization process of the entire system. This analysis is extremely important to check interactions between the detailed and simplified system or to properly develop robust controllers for power-electronic devices. In addition to that, the authors aim in including the implementation of the AC terminal voltage control in the STATCOM control system.

References

[1] N. Hingorani and L. Gyugyi, *Understanding FACTS, concepts and technology of flexible alternative current transmission system*, New York: IEEE Press, 2000.

[2] P. Kundur, N. J. Balu and M. G. Lauby, *Power system stability and control*, vol. 7, New York: McGraw-hill, 1994.

[3] J. H. Choq and J. J. Sanchez=Gasca, *Power system modeling, computation and control*, John Wiley & Sons, 2020.

[4] H. W. Dommel, *EMTP theory book*, Microtran Power System Analysis Corporation, 1996.

[5] A. S. Morched, J. H. Ottevangers and L. Marti, "Multi-port frequency dependent network equivalents for the EMTP", *IEEE Transactions on Power Delivery*, vol. 8, no. 3, Jul., pp. 1402-1412, 1993.

[6] N. Watson and J. Arrillaga, *Power Systems Electromagnetic Transients Simulation*, vol. 39, IET, 2003.

[7] N. G. Hingorani M. F. Burbery,"Simulation of AC system impedance in HVDC system studies", *IEEE Transactions on Power Apparatus and Systems*, vol. 5, May, pp.820-828, 1970.

[8] M. D. Heffernan, K. S. Turner, J. Arrillaga and C. P. Arnold, "Computation of ac-dc system disturbances. Part I: Interactive coordination of generator and convertor transient models", *IEEE Transactions on Power Apparatus and Systems*, vol. 11, Nov., pp. 4341-4348, 1981.

[9] R. Adapa and J. Reeve, "A new approach to dynamic analysis of AC networks incorporating detailed modeling of DC systems. Part II: Application to interaction of DC and weak AC systems", *IEEE Transactions on Power Delivery*, vol. 3, no. 4, Oct., pp.2012-2019, 1988.

[10] T. S. Theodoro, M. A. Tomim, A. C. S. de Lima and P. G. Barbosa, "A hybrid simulation tool for penetration studies of distributed generation in smartgrids", 2017 Brazilian Power Electronics Conference (COBEP), 2017, pp.1-7.

[11] T. S. Theodoro, M. A. Tomim, P. G. Barbosa, A. C. S. de Lima and M. T. Correia, "A flexible co-simulation framework for penetration studies of power electronics based renewable sources: A new algorithm for phasor extraction", *International Journal of Electrical Power & Energy Systems*, vol. 113, Dec., pp. 419-435, 2019.

[12] T. S. Theodoro, M. A. Tomim, P. G. Barbosa, A. C. S. de Lima and J. Santiago,"A Hybrid Simulation Tool for Distributed Generation Integration Studies", 2018 Power Systems Computation Conference (PSCC), 2018, pp. 1-8.

[13] Modelica Association, "Modelica Language", Available: `https://modelica.org/modelicalanguage.html`, [Accessed: July 8 2021].

[14] P. Fritzon, *Principles of Object-Oriented Modeling and Simulation with Modelica 3.3: A Cyber-Physical Approach*, 2nd Edition, Wiley-IEEE Press, 2014.

[15] P. M. Gibert, R. Losseau, A. Guironnet, P. Panciatici, D. Tromeur-Dervout and J. Erhel, "Use of the Sinusoidal Predictor Method within a Fully Separated Modeler/Solver Framework for Fast and Flexible EMT Simulations", SIMULTECH 2018 - 8th International Conference on Simulation and Modeling Methodologies, Technologies and Applications, pp. 34-43, 2018.

[16] Modelica Association Project, "Functional Mock-up Interface", Available: `https://fmi-standard.org/`, [Accessed: July 8 2021].

[17] M. Baudette, M. Castro, T. Rabuzin, J. Lavenius, T. Bogodorova and L. Vanfretti, "OpenIPSL: Open-instance power system library—update 1.5 to iTesla power systems library (iPSL): A modelica library for phasor time-domain simulations", *SoftwareX*, vol. 7, Jan., pp. 34-36, 2018.

[18] P. Rodriguez, R. Teodorescu, I. Candela, A. V. Timbus, M. Liserre and F. Blaabjerg, "New positive-sequence voltage detector for grid synchronization of power converters under faulty grid conditions", 2006 37th IEEE Power Electronics Specialists Conference, pp. 1-6, 2006.

[19] A. Yazdani and R. Iravani, *Voltage-sourced converters in power systems*, vol. 34, Hoboken, NJ: John Wiley & Sons, 2010.